JOURNAL OF PROTEOMICS 103 (2014) 153–169

Available online at www.sciencedirect.com

ScienceDirect

www.elsevier.com/locate/jprot

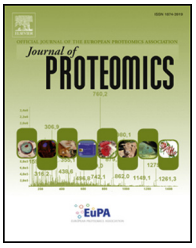

Quantitative proteomics reveals ER-α involvement in CD146-induced epithelial-mesenchymal transition in breast cancer cells

Qiqun Zeng[a,1], Peng Zhang[a,b,1], Zhenzhen Wu[a,b,1], Peng Xue[a], Di Lu[a], Zhongde Ye[a], Xinlei Zhang[a,b], Zechi Huang[a,b], Jing Feng[a], Lina Song[a], Dongling Yang[a], Taijiao Jiang[a,*], Xiyun Yan[a,*]

[a]Key Laboratory of Protein and Peptide Pharmaceuticals, CAS-University of Tokyo Joint Laboratory of Structural Virology and Immunology, Institute of Biophysics, Chinese Academy of Sciences, 15 Datun Road, Beijing 100101, China
[b]University of Chinese Academy of Sciences, 19A Yuquan Road, Beijing 100049, China

ARTICLE INFO

Article history:
Received 23 September 2013
Accepted 24 March 2014

Keywords:
Epithelial–mesenchymal transition
CD146
SILAC
Proteome
ER-α
Triple negative breast cancer

ABSTRACT

The cell adhesion molecule CD146 is a novel inducer of epithelial–mesenchymal transition (EMT), which was associated with triple-negative breast cancer (TNBC). To gain insights into the complex networks that mediate CD146-induced EMT in breast cancers, we conducted a triple Stable Isotope Labeling with Amino Acids in Cell Culture (SILAC), to analyze whole cell protein profiles of MCF-7 cells that had undergone gradual EMT upon CD146 expression from moderate to high levels. In this study, we identified 2293 proteins in total, of which 103 exhibited changes in protein abundance that correlated with CD146 expression levels, revealing extensive morphological and biochemical changes associated with EMT. Ingenuity Pathway Analysis (IPA) showed that estrogen receptor (ER) was the most significantly inhibited transcription regulator during CD146-induced EMT. Functional assays further revealed that ER-α expression was repressed in cells undergoing CD146-induced EMT, whereas re-expression of ER-α abolished their migratory and invasive behavior. Lastly, we found that ER-α mediated its effects on CD146-induced EMT via repression of the key EMT transcriptional factor Slug. Our study revealed the molecular details of the complex signaling networks during CD146-induced EMT, and provided important clues for future exploration of the mechanisms underlying the association between CD146 and TNBC as observed in the clinic.

Biological significance
This study used a proteomics screen to reveal molecular changes mediated by CD146-induced epithelial–mesenchymal transition (EMT) in breast cancer cells. Estrogen receptor

Abbreviations: SILAC, Stable Isotope Labeling with Amino Acids in Cell Culture; EMT, epithelial–mesenchymal transition; TNBC, ER⁻/PR⁻/ERBB⁻ triple-negative breast cancer; ER, estrogen receptor; ER-α, estrogen receptor-α; ER-β, estrogen receptor-β; RT-PCR, reverse transcription-PCR; WB, western blotting; IPA, Ingenuity Pathway Analysis; DAVID, the Database for Annotation, Visualization and Integrated Discovery; 2-DE, two-dimensional gel electrophoresis.

* *Corresponding authors at:* 15 Datun Road, Chaoyang District, Beijing 100101, China. Tel.: +86 10 6488 8583, +86 10 6488 8427; fax: +86 10 6488 8584, +86 10 6488 8427.
E-mail addresses: taijiao@moon.ibp.ac.cn (T. Jiang), yanxy@ibp.ac.cn (X. Yan).
[1] These authors contributed equally.

http://dx.doi.org/10.1016/j.jprot.2014.03.033
1874-3919/

(ER) was found to be the most significantly inhibited transcription regulator, which mediated its effects on CD146-induced EMT via repression of the transcriptional factor Slug. Elucidation of protein interaction networks and signal networks generated from 103 significantly changed proteins would facilitate future investigation into the mechanisms underlying CD146 induced-EMT in breast cancers.

1. Introduction

The term epithelial–mesenchymal transition (EMT) describes the biological process in which a polarized epithelial cell, distinguished by both cobblestone-like morphology and restricted cell motility, is converted into an elongated spindle-like shape mesenchymal cell with increased cell migratory and invasive capabilities [1]. Molecularly, EMT is characterized by the loss of the key epithelial marker E-cadherin and cytokeratin intermediated filaments, and a gain of N-cadherin-mediated inter-cell adhesion system and vimentin filaments. Originally identified as a mechanism essential for morphogenesis during embryonic development, more recently EMT has been implicated in cancer progression and metastasis. It is believed that a subset of primary epithelial tumor cells undergo EMT in the process of which they acquire enhanced cell motility and invasiveness, enabling them to initiate local invasion and distal metastasis [2].

The hallmark event of an EMT is the loss of the epithelial marker E-cadherin [3], which can be transcriptionally repressed by a series of transcription factors including Snail, Slug, Zeb, E47 and Twist. A number of signal pathways converge on these key transcription factors to regulate an EMT, such as TGF-β, Wnt and Notch signal pathways. Diverse growth factors and their corresponding tyrosine kinase receptors, including Met, FGF, IGF, EGF and PDGF family members, also play important roles in inducing EMT-like morphogenetic events [4]. In addition to the pathways triggered by these well-known membrane receptors, cell adhesion molecules and intracellular molecules have been described recently as inducers of EMT. For instance, L1-CAM induces EMT in epithelial breast cancer cells through disruption of E-cadherin-mediated adhesion junctions and promotion of β-catenin nuclear localization [5]. Due to the cooperation of multiple signaling pathways in an EMT process, the molecular events and signal networks activated by each individual EMT inducer are complex and remain poorly understood.

We recently identified another cell adhesion molecule, namely CD146, as a novel EMT inducer [6]. CD146, also known as MCAM, M-CAM and MUC18, is a member of the immunoglobulin superfamily. Originally identified as a melanoma-specific marker [7], CD146 has been found to play an important role in tumor angiogenesis [8,9] and tumor progression of several cancers, including melanoma [7], prostate cancer [10,11], epithelial ovarian cancer [12,13], lung adenocarcinomas [13,14], gastric cancer [15], mesothelioma [16,17] and breast cancer [6,18,19]. In our previous work, we found that overexpression of CD146 allows epithelial breast cancer cells to undergo EMT, which endows cells with migratory and invasive properties, and also induces stem cell-like properties. An orthotopic breast cancer mouse model showed that CD146-induced EMT promotes tumorigenesis and metastasis. Immunohistochemical analysis of 505 breast cancer samples further revealed that CD146 expression is significantly associated with high tumor grade, poor prognosis, ER-negative status and TNBC phenotype [6]. These results provided insights into the underlying mechanisms by which the RhoA/Slug axis mediates CD146-induced EMT, and initiated experimental examination of additional essential mechanisms and the exact function of CD146 in this process.

Here, we have carried out an in-depth triple-SILAC-labeling comparative proteomic analysis of the breast cancer cell line MCF-7 that underwent gradual CD146-mediated EMT, whereby CD146 was expressed at moderate to high levels. Analysis of whole cell protein expression profiles using MaxQuant identified novel proteins with altered abundances that correlated with differences in CD146 expression. The identified proteins provided clues to generate complex interaction and signaling networks, and possible transcriptional regulators that mediate CD146-induced EMT. For all proteins exhibiting altered abundances, gene expression levels were examined via microarray mRNA expression analysis. Furthermore, an in vitro system was employed to confirm the functional outcomes of the key transcription regulator during the CD146-induced EMT process. Taken together, our study revealed that breast cancer cells with CD146 overexpression underwent extensive morphological and biochemical changes associated with EMT, and provided evidences for further exploration of the mechanisms underlying the association between CD146 and clinical TNBC.

2. Experimental procedure

2.1. Cell culture and SILAC labeling

MCF-7 (American Type Culture Collection, USA) derived cell lines, including vector control MCF-7-Mock (Mock cells) as well as CD146-overexpressing clones MCF-7-B10 (B10 cells) and MCF-7-A5 (A5 cells) were maintained in Minimum Essential Media (MEM, Invitrogen) supplemented with 10% fetal bovine serum (Invitrogen). To generate triple encoding SILAC conditions, normal MEM medium deficient in arginine and lysine (Invitrogen) was supplemented with stable isotope-encoded arginine and lysine (Cambridge Isotope Laboratories, Inc.). For Mock cells with "Light" labeling, L-[$^{12}C_6$,$^{14}N_4$] arginine (Arg0) and L-[$^{12}C_6$,$^{14}N_2$] lysine (Lys0) were used; for B10 cells with "Medium" labeling, L-[$^{13}C_6$] arginine (Arg6) and L-[$^{2}H_4$] lysine (Lys4) were used; for A5 cells with "Heavy" labeling, L-[$^{13}C_6$,$^{15}N_4$] arginine (Arg10) and L-[$^{13}C_6$,$^{15}N_2$] lysine (Lys8) were used. Final concentrations of arginine and lysine were 84 mg/ml and 146 mg/ml in MEM medium, respectively. Each cell line was grown in all of the appropriate media over the period of 6 generations. For each SILAC condition, MEM medium was supplemented with 10% dialyzed fetal bovine serum using 10-kDa cutoff tubing (Invitrogen), and 1% streptomycin (10 mg/ml)/penicillin (10,000 units/ml).

2.2. Immunofluorescence microscopy

Cells were cultured on round coverslips in 6-well plates until they reached 80% confluence. Then cells were washed twice with PBS buffer, fixed with 4% paraformaldehyde for 15 min, permeabilized with 0.1% Triton/PBS for 3 min at room temperature, and blocked for 30 min using 5% normal goat serum. Coverslips were subsequently incubated with anti-CD146 (AA1 ascites, generated by our lab), anti-E-cadherin (Abcam), anti-vimentin (Sigma) or anti-ER-α (Santa Cruz) antibodies for 1 h at 37 °C, followed by incubation with an Alex Fluor 488 $(Fab)_2$ fragment of goat anti-mouse or rabbit IgG (H + L) (Invitrogen) for 45 min at 37 °C. Finally, cells were analyzed by confocal laser scanning microscopy (FV-1000, Olympus, Japan).

2.3. Western blot

Cells were lysed in RIPA lysis buffer (150 mM NaCl, 1 mM EDTA, 50 mM Tris, pH 8.0, 10% glycerol, 1% Triton X-100, 1 mM phenylmethylsulfonyl fluoride (PMSF), and 25 μg/ml aprotinin) and were transferred onto nitrocellulose membranes (Millipore) following separation by 10% SDS-PAGE. Membranes were blocked with 5% nonfat dry milk in PBS for 1 h, followed by incubation with the appropriate primary antibodies for 1 h, and HRP-conjugated anti-mouse or anti-rabbit antibodies (GE Healthcare) incubation for 45 min at room temperature. Enhanced chemiluminescence (Pierce) was used to detect the presence of specific immunoreactive proteins.

2.4. Sample preparation

Cells were washed three times with PBS buffer and then lysed by sonication in lysis buffer (7 M urea, 2 M thiourea, 1 mM Complete Mini EDTA-free Cocktail (Roche)). The lysate was then centrifuged for 15 min at 20,000 *g* and the supernatant was transferred into a new tube. Protein concentration was determined by Bradford assay (Pierce). Proteins were reduced (10 mM dithiothreitol, 45 min) and alkylated (30 mM iodoacetamide, 45 min at room temperature in the dark). Excess iodoacetamide was removed by 40 mM DTT at room temperature. Lys-C was added in a 1:75 (w/w) ratio and incubated for 4 h at 37 °C. Samples were diluted four times with 50 mM ammonium bicarbonate buffer. Sequencing-grade trypsin (Promega) was added in a 1:100 (w/w) ratio and the incubation was carried out overnight at 37 °C.

2.5. LC–MS analysis

LC–MS was performed as reported by John Yates using LTQ orbitrap MS (Thermo Fisher Scientific, Waltham, USA) [20,21]. 100 μg digested peptides were injected into a self-made biphasic capillary column 200 μm i.d. packed with 3 cm of a C18 resin (Sunchrom 5 μm, Germany) and 3 cm of a strong cation exchange resin (Luna 5 μm SCX 100A, Phenomenex). The used buffers were 0.1% FA (buffer A), 100% ACN/0.1% FA (buffer B), and 800 mM ammonium acetate 5% ACN/0.1% FA (buffer C). The peptide effluents of the biphasic column in each step were directed onto a 15 cm C 18 analytical column (75 μm i.d.) with 500 nl flow rate. The biphasic column was firstly desalted with buffer A and then eluted using an 11-step salt gradient ranging from 0 to 800 mM ammonium acetate. The specific steps were as follows: step 1 involved 0–80% mobile phase B for 100 min. Steps 2 to 10 have the following profile, and in this order: 100% mobile phase A for 3 min, X% mobile phase C for 10 min, 0–10% mobile phase B in gradient for 5 min, 10%–35% mobile phase B in gradient for 77 min, 35%–100% mobile phase B for 10 min, and 80% mobile phase B of the balanced column for 10 min. X% mobile phase C represents the concentration of ammonium acetate of 5%, 10%, 15%, 20%, 30%, 40%, 50%, 60%, 80% and 100%. Nano-ESI was accomplished with a spray voltage of 2.0 kV and a heated capillary temperature of 200 °C. Mass spectra were acquired in a data-dependent manner. One full MS scan (300–1800) in the orbitrap was followed by five MS/MS scans on the five most intense ions selected from the MS spectrum in LTQ. The orbitrap analyzer resolution was set at 60,000 (at m/z = 400). Charge state screening was enabled for +2, +3, +4 and above. All MS/MS spectra were acquired using the following parameters: normalized collision energy, 35%; ion selection threshold maximum injection time, 150 ms; dynamic exclusion time, 120 s; exclusion list size, 300.

2.6. Data analysis

Raw mass spectrometric data were analyzed using MaxQuant software (version 1.2.2.5) [22,23]. A false discovery rate (FDR) of 0.01 for proteins and peptides, and a minimum peptide length of 5 amino acids were required. MS/MS spectra were searched by Andromeda against the IPI human database (version 3.85) (containing 84,808 entries) combined with 262 common contaminants (http://www.maxquant.org/downloads.htm) and concatenated with the reversed versions of all sequences. The minimum number of peptides or MS/MS required to positively identify a protein was one; the minimum number of quantitative values from MS pairs required to provide a statistically valid ratio of a protein was two. For the Andromeda search trypsin allowing for cleavage N-terminal to proline was chosen as enzyme specificity. Cysteine carbamidomethylation was selected as a fixed modification, while protein N-terminal acetylation and methionine oxidation were selected to serve as variable modifications. MaxQuant determined the SILAC state of peptides by the mass differences between SILAC peptide pairs. This information was used to perform searches with Arg6 and Lys4 or Arg10 and Lys8 as variable modifications. At maximum, two missed cleavages and three labeled amino acids were allowed. Initial mass deviation of precursor ion was up to 7 ppm, and mass deviation for fragment ions was 0.5 units on the m/z scale. Quantification in MaxQuant was performed as described previously [23]. The "Requantify" option was enabled, which in elect integrates noise levels for undetected SILAC partners, in order to estimate a lower limit on the SILAC ratio.

2.7. GeneChip expression analysis

Total RNA was extracted from 5×10^6 MCF-7 cells using TRIZOL reagent (Invitrogen) following the instructions of the manufacturer, and checked RIN numbers as a measure of RNA integrity using the Agilent Bioanalyzer 2100 system (Agilent, Santa Clara, CA, USA). High-quality total RNA was further purified using the RNeasy micro kit (Cat #74004, QIAGEN, GmBH, Germany) and RNase-Free DNase Set (Cat #79254, QIAGEN, GmBH, Germany).

RNA was labeled and hybridized to the Affymetrix GeneChip® Human Genome U133 Plus 2.0 Arrays (Affymetrix/Millenium, Santa Clara, CA, USA). To obtain biotinylated cRNA, total RNA was amplified, labeled and purified using GeneChip 3′IVT Express Kit (Cat #901229, Affymetrix, Santa Clara, CA, USA) following the manufacturer's instructions. Array hybridization and washes were performed using GeneChip® Hybridization, Wash and Stain Kit (Cat #900720, Affymetrix, Santa Clara, CA, USA) in Hybridization Oven 645 (Cat #00-0331-220 V, Affymetrix, Santa Clara, CA, USA) and Fluidics Station 450 (Cat #00-0079, Affymetrix, Santa Clara, CA, USA) following the manufacturer's instructions. Slides were scanned by GeneChip® Scanner 3000 (Cat #00-00212, Affymetrix, Santa Clara, CA, USA) and Command Console Software 3.1 (Affymetrix, Santa Clara, CA, USA) with default settings. Raw data were normalized using the MAS 5.0 algorithm, Gene Spring Software 11.0 (Agilent, Santa Clara, CA, USA).

2.8. RNA isolation and reverse transcription-PCR (RT-PCR)

TRIZOL reagent was used to isolate total RNA from cultured cells. 2 μg of RNA was subjected to cDNA synthesis by Superscript III reverse transcriptase (Invitrogen). The PCR reaction was then performed using 1 μl cDNA and a pair of primers specific for each gene. PCR products were visualized on a 1% agarose gel by staining with EB and photographed with a gel imaging system (Bio-Rad Laboratories). The sequences of the PCR primers are as follows: CD146, Forward 5′-GCT GCC CAG TGG GAA CCA CA-3′; Reverse 5′-ATC ATG GTG TCC AAG TTC CAG GC-3′. ER-α, Forward 5′-CAC TCA ACA GCG TGT CTC CGA-3′; Reverse 5′-CCA ATC TTT CTC TGC CAC CCT G-3′. GAPDH, Forward 5′-AGG TCG GAG TCA ACG GAT TTG-3′; Reverse 5′-GTG ATG GCA TGG ACT GTG GT-3′.

2.9. Plasmid construction and transfection

The coding sequence of human ER-α was cloned in-frame into the EcoRI and BamH I sites of the plasmid p3 × FLAG-cmv-14. Vectors were transfected into MCF-7 A5 cells using Fugen HD reagent according to the manufacturer's instructions (Roche).

2.10. Transwell invasion assay

Cell migration was assayed using Transwell (8 μm pore size; Corning Costar) pre-coated with Matrigel (2.5 mg/ml, BD Biosciences). 5000 cells were resuspended in serum free medium and transferred into upper chamber of each well. Lower chambers contained fresh medium containing 10% fetal bovine serum as chemoattraction. After incubation at 37 °C overnight, cells remaining at the upper surface of the membrane were removed using a swab, whereas cells that invaded to the lower membrane surface were fixed with 4% paraformaldehyde and stained with Crystal violet solution. The number of cells invading through the filter was photographed and counted.

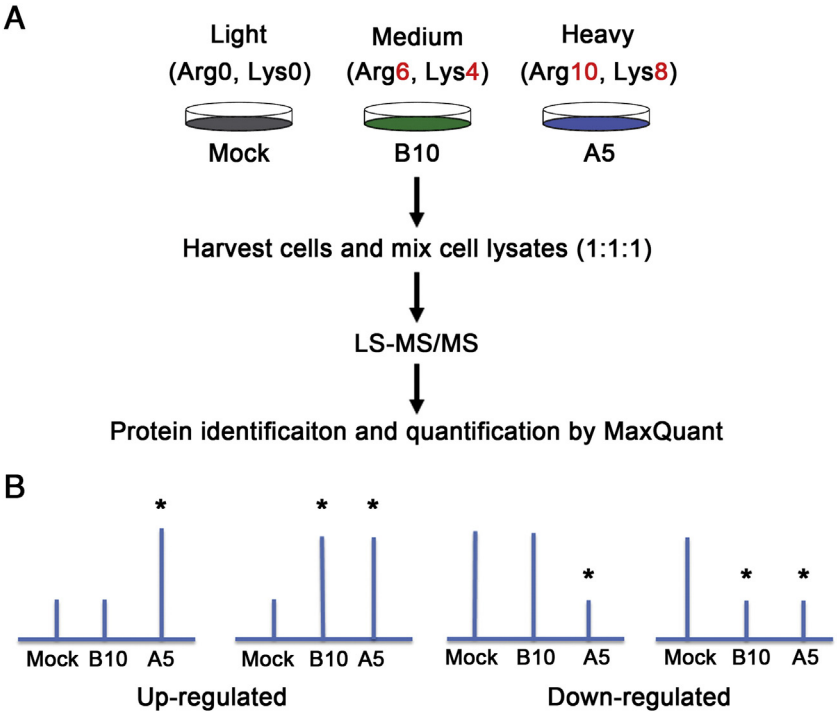

Fig. 1 – Strategy to explore the cellular signaling networks involved in CD146-induced EMT. (A) Three SILAC-labeled condition. Mock cells, light-labeling (Arg0, Lys0); B10 cells, medium-labeling (Arg6, Lys4); A5 cells, heavy-labeling (Arg10, Lys8). (B) Four major response patterns associated with CD146 expression levels as reflected in SILAC spectra. The "up-regulated trend" includes proteins significantly up-regulated in A5 cells alone and in both B10 and A5 cells; the "down-regulated trend" includes proteins significantly down-regulated in A5 cells alone and in both B10 and A5 cells. *, significance B value (intensity-dependent P value) calculated by MaxQuant ≤ 0.01, as compared with Mock cells.

3. Results

3.1. CD146 overexpression induces EMT in breast cancer cells

Our previous study showed that MCF-7 cells that were stably transfected with CD146 underwent EMT, revealing that CD146 is a previously unknown inducer of EMT in breast cancer cells [6]. In this study, vector control clone MCF-7-Mock (Mock), as well as CD146-expressing clones MCF-7-B10 (B10) and MCF-7-A5 (A5) were assessed for characteristic changes associated with EMT. As shown in Fig. S1A, Mock cells with a CD146-negative status maintained their cobblestone-like morphology, exhibiting strong intercellular contact. In contrast, A5 cells with the highest CD146 expression exhibited an elongated spindle-like morphology as well as pronounced cellular scattering. B10 cells that expressed CD146 at moderate levels resembled a transitional phenotype between Mock and A5 cells. In addition, an immunofluorescent assay showed that the epithelial marker E-cadherin was decreased and the mesenchymal maker vimentin was gradually increased in B10 and A5 cells when compared to levels observed in Mock cells (Fig. S1B). These changes of EMT markers were further confirmed by immunoblotting (Fig. S1C). More importantly, increased expression of CD146, especially in A5 cells, significantly promoted cell invasion through Matrigel, whereas few invading cells were observed in Mock cells (Fig. S1D).

A

B10/Mock(M/L) \ A5/Mock(H/L)	Up	medium	Down	Sum
Up	6	46	0	52
medium	53	2075	36	2164
Down	4	65	8	77
Sum	63	2186	44	2293

B

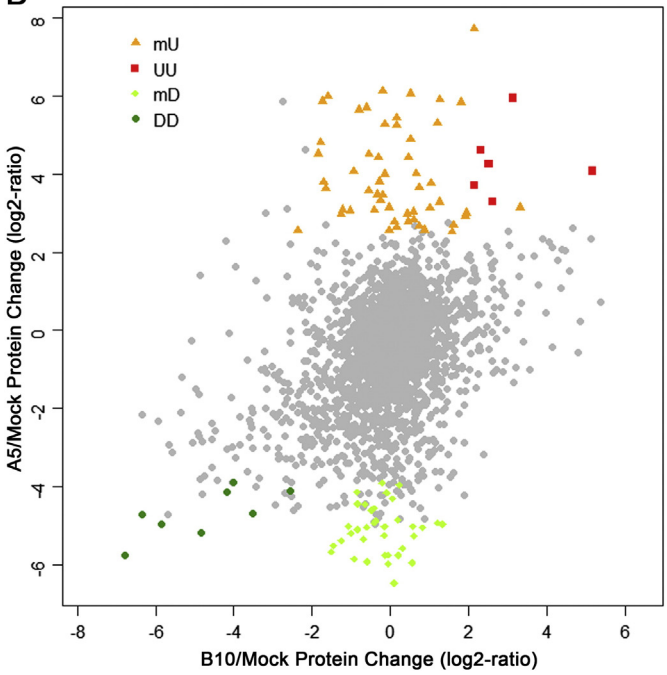

Fig. 2 – MaxQuant analysis identifies proteins with altered abundance in CD146-induced EMT. (A) Summary of nine different protein expression patterns. The significantly changed proteins were defined by significance B. "Up" represents "up-regulated", log2-ratio > 0 and significance B value ≤ 0.01, "Down" represents "down-regulated", log2-ratio < 0 and significance B value ≤ 0.01 and "medium" represents "unchanged" and significance B value > 0.01. (B) Distribution of differently expressed proteins correlated with CD146 expression level in breast cancer cells. Compared with Mock cells, proteins indicated as orange triangles were up-regulated only in A5 cells (B10/Mock medium + A5/Mock Up, mU), proteins indicated as red squares were up-regulated both in B10 and in A5 cells (B10/Mock Up + A5/Mock Up, UU), proteins indicated as yellow–green diamonds were down-regulated only in A5 cells (B10/Mock medium + A5/Mock Down, mD), proteins indicated as green circles were down-regulated both in B10 and in A5 cells (B10/Mock Down + A5/Mock Down, DD). Proteins indicated as gray dots were the proteins for which no significant changes were observed, or whose expression did not correlated with CD146 expression pattern.

Table 1 – Selected proteins that were differently expressed during CD146-induced EMT.

Gene name	Protein name	SILAC protein ratios (log2)		Microarray fold change (log2)		Pattern
		M/L [a]	H/L [b]	M/L [a]	H/L [b]	
DHRS9	Dehydrogenase/reductase SDR family member 9	3.1503	5.9396	0.9600	5.4050	UU
AKR1B1	Aldose reductase	2.1478	3.7042	6.8733	4.5105	UU
MGST3	Microsomal glutathione S-transferase 3	2.3156	4.6122	1.9465	3.4021	UU
MSN	Moesin	2.5248	4.2494	10.9832	5.9426	UU
IGF2BP2	Insulin-like growth factor 2 mRNA-binding protein 2	2.6292	3.2872	3.8849	7.8940	UU
RCN1	Reticulocalbin-1	5.1680	4.0759	5.6921	−1.7602	UU
SERPINB8	Serpin B8	−0.7966	5.6386	−0.5953	4.6458	mU
S100A4	Protein S100-A4	−1.5816	5.9899	−2.0380	6.6345	mU
EVL	Ena/VASP-like protein	−1.7745	4.7980	−1.2277	−2.4297	mU
EXOSC1	Exosome complex component CSL4	0.5293	6.0559	−0.1373	6.4361	mU
ANXA1	Annexin A1	−0.5988	5.6929	−0.4507	1.5997	mU
PRKCDBP	Protein kinase C delta-binding protein	−0.1889	6.1263	−1.8594	8.0401	mU
CD44	CD44 antigen	−1.8494	4.5108	0.8654	3.7211	mU
SORBS3	Vinexin	−1.7274	5.8594	−0.6275	3.1873	mU
SNCG	Gamma-synuclein	0.1650	5.4414	−0.2360	3.8941	mU
ARHGAP26	Rho GTPase-activating protein 26	2.1544	7.7215	0.7632	4.5270	mU
PTGR1	Prostaglandin reductase 1	−2.3614	2.5521	−4.4143	−0.3219	mU
FAM114A2	Protein FAM114A2	−0.9291	4.0661	0.5862	0.0119	mU
MCAM	Cell surface glycoprotein MUC18	0.1718	5.2471	1.6081	3.8403	mU
CAPG	Macrophage-capping protein	−1.6552	3.6211	−1.2036	9.3288	mU
HTRA1	Serine protease HTRA1	−0.1453	5.2657	0.9296	0.9995	mU
ANXA8	Annexin A8	−1.7013	3.7808	−3.0529	1.9247	mU
HMSD	Serpin-like protein HMSD	0.5151	4.8907	NA	NA	mU
HEPH	Hephaestin	−0.2955	4.4267	0.3646	7.9957	mU
IGBP1	Immunoglobulin-binding protein 1	−0.3333	3.4760	−0.7264	−4.7027	mU
HMGA2	High mobility group protein HMGI-C	1.8020	5.8292	0.0606	5.0252	mU
HMGA1	High mobility group protein HMG-I/HMG-Y	−1.2526	2.9794	1.5346	4.7883	mU
CRYAB	Alpha-crystallin B chain	−0.5370	4.5050	1.1090	10.4245	mU
BCAT1	Branched-chain-amino-acid aminotransferase, cytosolic	1.2725	5.9013	4.5796	10.7317	mU
VIM	Vimentin	1.2033	5.3044	6.8544	12.0688	mU
ITGA3	Integrin alpha-3	−1.2206	3.0904	−2.1203	2.6616	mU
DPYSL3	Dihydropyrimidinase-related protein 3	−1.0274	3.0569	1.6320	6.0411	mU
NDRG1	Protein NDRG1	−0.1331	3.9928	1.3806	0.3493	mU
ABCB1	Multidrug resistance protein 1	0.4707	4.4217	0.4357	2.0858	mU
ABCB4	Multidrug resistance protein 3	0.4707	4.4217	−0.6412	4.6187	mU
GLIPR2	Golgi-associated plant pathogenesis-related protein 1	0.6706	4.0163	0.7661	0.9433	mU
TNS1	Tensin-1	−0.5526	3.5739	0.4626	7.5523	mU
EML2	Echinoderm microtubule-associated protein-like 2	−0.2679	3.8045	0.2947	6.4576	mU
ITGA6	Integrin alpha-6	0.7445	3.6439	1.6133	2.3327	mU
TUBB6	Tubulin beta-6 chain	−0.2552	3.3219	0.2611	−6.2433	mU
PIR	Pirin	−0.0222	3.1423	1.8418	0.7530	mU
DGKA	Diacylglycerol kinase alpha	−0.4022	3.0784	0.1890	5.8408	mU
DGKB	Diacylglycerol kinase beta	−0.4022	3.0784	1.0574	6.2691	mU

EHD2	EH domain-containing protein 2	−0.0291	2.5486	0.9806	2.0256	mU
EHD4	EH domain-containing protein 4	−0.0291	2.5486	0.0938	0.6595	mU
RTN4	Reticulon-4	0.1609	2.6347	−0.6255	4.0694	mU
TLN1	Talin-1	0.1165	2.7753	0.4580	4.3390	mU
LRP1	Prolow-density lipoprotein receptor-related protein 1	0.5902	3.0364	−0.1722	2.5387	mU
CAPN2	Calpain-2 catalytic subunit	1.0451	3.7599	0.0360	1.9381	mU
KTN1	Kinectin	0.8816	2.5715	0.3172	4.9376	mU
CPD	Carboxypeptidase D	1.0220	3.1239	1.2136	5.3979	mU
GLUD1	Glutamate dehydrogenase 1, mitochondrial	0.4535	2.7915	0.8047	−3.0362	mU
GLUD2	Glutamate dehydrogenase 2, mitochondrial	0.4535	2.7915	0.3353	2.1039	mU
ZNF598	Zinc finger protein 598	0.4439	2.9802	0.8034	3.8897	mU
CKAP4	Cytoskeleton-associated protein 4	0.6014	2.8301	0.5064	0.1389	mU
TUBB2A	Tubulin beta-2A chain	1.2549	3.2775	0.9721	5.4901	mU
TUBB2B	Tubulin beta-2B chain	1.2549	3.2775	0.9721	5.4901	mU
ARL6IP5	PRA1 family protein 3	0.7327	2.6680	1.0812	−4.0565	mU
HK2	Hexokinase-2	1.9399	3.0020	4.8978	4.8646	mU
PRPS1	Ribose-phosphate pyrophosphokinase 1	1.9231	2.9077	1.9945	0.7625	mU
PRPS1L1	Ribose-phosphate pyrophosphokinase 3	1.9231	2.9077	2.0633	6.7224	mU
GCLM	Glutamate–cysteine ligase regulatory subunit	1.6148	2.6846	1.5512	−1.1056	mU
CYB5R3	NADH-cytochrome b5 reductase 3	1.5811	2.5261	1.1757	0.3372	mU
IGF2BP3	Insulin-like growth factor 2 mRNA-binding protein 3	3.3250	3.1471	1.5999	4.2568	mU
PLK1	Serine/threonine-protein kinase PLK1	1.2101	−4.9258	0.1835	3.4478	mD
SCRN1	Secernin-1	−0.8396	−4.1405	−0.6811	−3.3555	mD
APEX1	DNA-(apurinic or apyrimidinic site) lyase	−0.8267	−4.4391	−0.5111	−2.8552	mD
TK1	Thymidine kinase, cytosolic	−0.2057	−3.9083	−1.1119	−2.3718	mD
DLST	Dihydrolipoyllysine-residue succinyltransferase component of 2-oxoglutarate dehydrogenase complex, mitochondrial	−0.8293	−5.0930	−1.0032	−3.2990	mD
DBI	Acyl-CoA-binding protein	−1.2443	−5.3808	−0.8163	−7.1380	mD
COX4I1	Cytochrome c oxidase subunit 4 isoform 1, mitochondrial	0.2378	−3.9546	−0.3067	−4.3688	mD
PPP2R4	Serine/threonine-protein phosphatase 2A activator	−0.6353	−4.4422	−1.1691	−0.3722	mD
SH3BGRL	SH3 domain-binding glutamic acid-rich-like protein	−1.4509	−5.5195	−0.1898	−9.9658	mD
COX5B	Cytochrome c oxidase subunit 5B, mitochondrial	−0.4013	−4.9258	−0.0950	−2.5204	mD
SLC7A5	Large neutral amino acids transporter small subunit 1	−1.0613	−5.0162	−1.3492	−6.2002	mD
C19orf10	UPF0556 protein C19orf10	−0.0833	−4.1559	1.0032	−0.3675	mD
REEP5	Receptor expression-enhancing protein 5	−1.5019	−5.6657	−1.2112	−2.9203	mD
FAM82B	Regulator of microtubule dynamics protein 1	−0.9968	−5.2002	−0.6244	−3.6153	mD
DIDO1	Death-inducer obliterator 1	−0.5888	−5.9214	−1.7070	−4.3306	mD
RSL1D1	Ribosomal L1 domain-containing protein 1	−0.4150	−4.5598	0.5310	−3.4691	mD
PRDX2	Peroxiredoxin-2	0.0595	−4.3133	−0.1178	−6.6439	mD
CHMP4B	Charged multivesicular body protein 4b	−0.1504	−5.2598	−0.2928	0.0712	mD
PDCL3	Phosducin-like protein 3	−0.6746	−5.3452	−1.0887	−8.9658	mD
PEBP1	Phosphatidylethanolamine-binding protein 1	−0.5942	−5.0303	−0.2971	−5.0637	mD
EBP	3-beta-hydroxysteroid-Delta(8),Delta(7)-isomerase	0.1941	−4.8489	−0.1269	−4.1203	mD
FAM82A2	Regulator of microtubule dynamics protein 3	−0.3642	−4.8783	−0.2526	−3.5113	mD
MARCKS	Myristoylated alanine-rich C-kinase substrate	−0.1357	−5.0209	−0.0325	−3.6439	mD
METAP2	Methionine aminopeptidase 2	−0.9159	−5.8531	1.5935	−5.0637	mD
NUBP2	Cytosolic Fe–S cluster assembly factor NUBP2	−0.1319	−5.7563	−1.3963	−0.9252	mD
NDUFA7	NADH dehydrogenase [ubiquinone] 1 alpha subcomplex subunit 7	−0.0423	−5.9748	0.8944	−0.1701	mD

(continued on next page)

Table 1 (*continued*)

Gene name	Protein name	SILAC protein ratios (log2)		Microarray fold change (log2)		Pattern
		M/L [a]	H/L [b]	M/L [a]	H/L [b]	
CDV3	Protein CDV3 homolog	−0.0518	−5.7486	0.1827	−3.7879	mD
TBCA	Tubulin-specific chaperone A	0.8326	−5.0445	0.3649	−3.6331	mD
COPS6	COP9 signalosome complex subunit 6	0.3235	−5.5804	−0.4951	−3.1494	mD
MRPL21	39S ribosomal protein L21, mitochondrial	0.5795	−5.0209	−0.0106	0.4770	mD
RBM3	Putative RNA-binding protein 3	0.6120	−5.2653	−0.0106	0.4770	mD
BOP1	Ribosome biogenesis protein BOP1	0.2134	−5.7563	0.4535	−0.9415	mD
HINT1	Histidine triad nucleotide-binding protein 1	0.5725	−5.9479	0.5644	0.8237	mD
MRE11A	Double-strand break repair protein MRE11A	1.3435	−4.9568	1.7089	−3.1090	mD
ABHD14B	Abhydrolase domain-containing protein 14B	0.1074	−6.4675	−0.1657	1.4366	mD
LGALS3	Galectin-3	−6.3452	−4.7217	−4.9885	−0.5698	DD
HSPB1	Heat shock protein beta-1	−5.8448	−4.9523	−3.7293	−7.8954	DD
AGR2	Anterior gradient protein 2 homolog	−4.0000	−3.8762	−11.7027	−8.9658	DD
CSRP1	Cysteine and glycine-rich protein 1	−6.7959	−5.7563	−3.7819	−0.6719	DD
ZNF548	Zinc finger protein 548	−4.8201	−5.1792	0.8344	2.1988	DD
CTSD	Cathepsin D	−4.1714	−4.1405	−6.7331	−3.7046	DD
EEF1A2	Elongation factor 1-alpha 2	−3.5129	−4.6878	−3.4173	−3.1469	DD
TST	Thiosulfate sulfurtransferase	−2.5522	−4.1078	−2.7103	−4.6259	DD

[a] B10/Mock.
[b] A5/Mock.

3.2. Strategy to explore the cellular signaling networks involved in CD146-induced EMT

To gain insight into the complex networks and novel mechanisms during CD146-induced EMT, we performed a proteomics analysis of Mock, B10 and A5 cells under triple-SILAC conditions. A schematic diagram of the experimental design was shown in Fig. 1A. Mock cells were light-labeled (Arg0, Lys0) and served as control; B10 cells were medium-labeled (Arg6, Lys4) and A5 cells were heavy-labeled (Arg10, Lys8). In this assay, we focused on proteins with statistically significant changes in expression associated with CD146 expression levels in these three cells, including the "up-regulated trend" and the "down-regulated trend" (Fig. 1B). Compared with Mock cells, proteins significantly up-regulated in A5 cells alone and in both B10 and A5 cells were included in the "up-regulated trend". Similarly, proteins significantly down-regulated in A5 cells alone and in both B10 and A5 cells were included in the "down-regulated trend". Additionally, RNAs were extracted from labeled Mock, B10 and A5 cells and subjected to Affymatix GeneChip analysis, for comparison with their corresponding protein expression profiles.

3.3. MaxQuant analysis identifies proteins with altered abundance in CD146-induced EMT

Mass spectrometric data were processed in MaxQuant. Respectively, 2344 proteins were identified for medium-labeled B10 cells, and 2338 proteins in heavy-labeled A5 cells, as compared to light-labeled Mock cells. In total, 2293 proteins were quantified in these three samples, and were processed for further analysis. Details of peptide and protein identification and quantification are shown in Supplementary Tables S1 and S2. The histograms of the changes in protein expression upon CD146 overexpression for all quantified proteins were shown in Fig. S2. The majority of proteins had log2 ratio between −1 and 1, indicating that most proteins remained unchanged upon CD146 overexpression, especially in B10 cells with moderate CD146 expression.

To define robust biological responses, we set a conservative significant cutoff of significance B value ≤ 0.01, which was calculated by Perseus (version 1.2.0.16) for proteins. After comparison with Mock cell protein levels, proteins in B10 cells were first grouped into three categories, namely "Up" (representing "up-regulated", log2-ratio > 0 and significance B value ≤ 0.01), "Down" (representing "down-regulated", log2-ratio < 0 and significance B value ≤ 0.01) and "medium" (representing "unchanged", significance B value > 0.01). Similarly, proteins in A5 cells were grouped into identical three categories. As a result, nine response patterns were defined, and quantification results were summarized as shown in Fig. 2A. Of these, "B10/Mock medium + A5/Mock **U**p, **mU**" pattern and "B10/Mock **U**p + A5/Mock **U**p, **UU**" pattern were included into the "up-regulated trend" group as shown in Fig. 1B, with 59 proteins in total. Similarly, "B10/Mock **m**edium + A5/Mock **D**own, **mD**" pattern and "B10/Mock **D**own + A5/Mock **D**own, **DD**" pattern were included into the "down-regulated trend" group, with a total of 44 proteins. Detailed information for the 103 identified proteins was listed in Table 1. Other response patterns (DU, Dm, Um and UD) did not correlate with CD146 expression in these three cells, probably due to individual clone differences. 2075 (90.4%) proteins (mm pattern) did not significantly change in abundance or could not be quantified with respect to peptide abundance.

Importantly, we observed upregulation of multiple markers associated with mesenchymal function and recruitment, including Annexin A1 (−0.6, 5.7, mU), CD44 (−1.8, 4.5, mU), moesin (2.5, 4.2, UU), integrin α-3 (−1.2, 3.1, mU), integrin α-6 (0.7, 3.6, mU), S100A4 (−1.6, 6.0, mU), HMGI-C (1.8, 5.8, mU) and the well-known EMT marker vimentin (1.2,5.3, mU) (Table 1), providing a robust positive control for our SILAC analysis. Furthermore, we performed an enrichment analysis with the 103 identified proteins using the Ingenuity Pathway Analysis (IPA) approach, to assist functional interpretation of the protein data sets. As shown in Fig. S3, the significantly associated biological functions included cell death, cell-to-cell signaling and interaction, cancer, tissue development, amino acid metabolism, cellular movement and cell morphology. The identification of these particular groups mirrors the extensive morphological and biochemical changes associated with EMT. Meanwhile, the significantly associated canonical pathways involved glutamate metabolism, FAK signaling, integrin signaling, Paxilin signaling, as well as ERK/MAPK signaling. Enrichment of these pathways indicates a likely role of CD146 in tumor cell metabolism and tumor cell adhesion.

3.4. Changes in mRNA transcript levels of significantly changed genes mirror changes in protein levels

To ascertain the correlation between transcript and proteins with altered abundances during CD146-induced EMT, we performed mRNA expression analysis. Selected probe information was extracted from the complete microarray data set, and correlation analysis was performed. Of the 103 identified proteins listed in Table 1, the Pearson correlation coefficient between mRNA and protein change indicated that both the direction and magnitude of changes in expression levels of most of the detected proteins were similar ($r > 0.7$). In addition, our microarray data provided information for proteins that could not be detected or quantified in our SILAC analysis. For example, several well-known epithelial markers were found to be down-regulated during CD146-induced EMT, including E-cadherin, desmoglein-2, cytokeratin 8, cytokeratin 19 and claudin 4 (data not shown).

3.5. Functional protein complexes in CD146-induced EMT

To better understand the overall influence of CD146-induced EMT on cellular signaling networks, we looked for protein interactions among the 103 identified proteins. To this end, we chose the "Search Tool for the Retrieval of Interacting Genes/Proteins" (STRING) database, which is constructed on the basis of both physical and functional interactions. Several interaction groups were immediately apparent (Fig. 3). For instance, the CD146 core group included MCAM (CD146), CD44, moesin and other proteins, clustered in the center of the interaction map. Gene Ontology enrichment analysis by DAVID showed that these proteins were significantly involved in cell adhesion, which is a characteristic cellular program involved in the

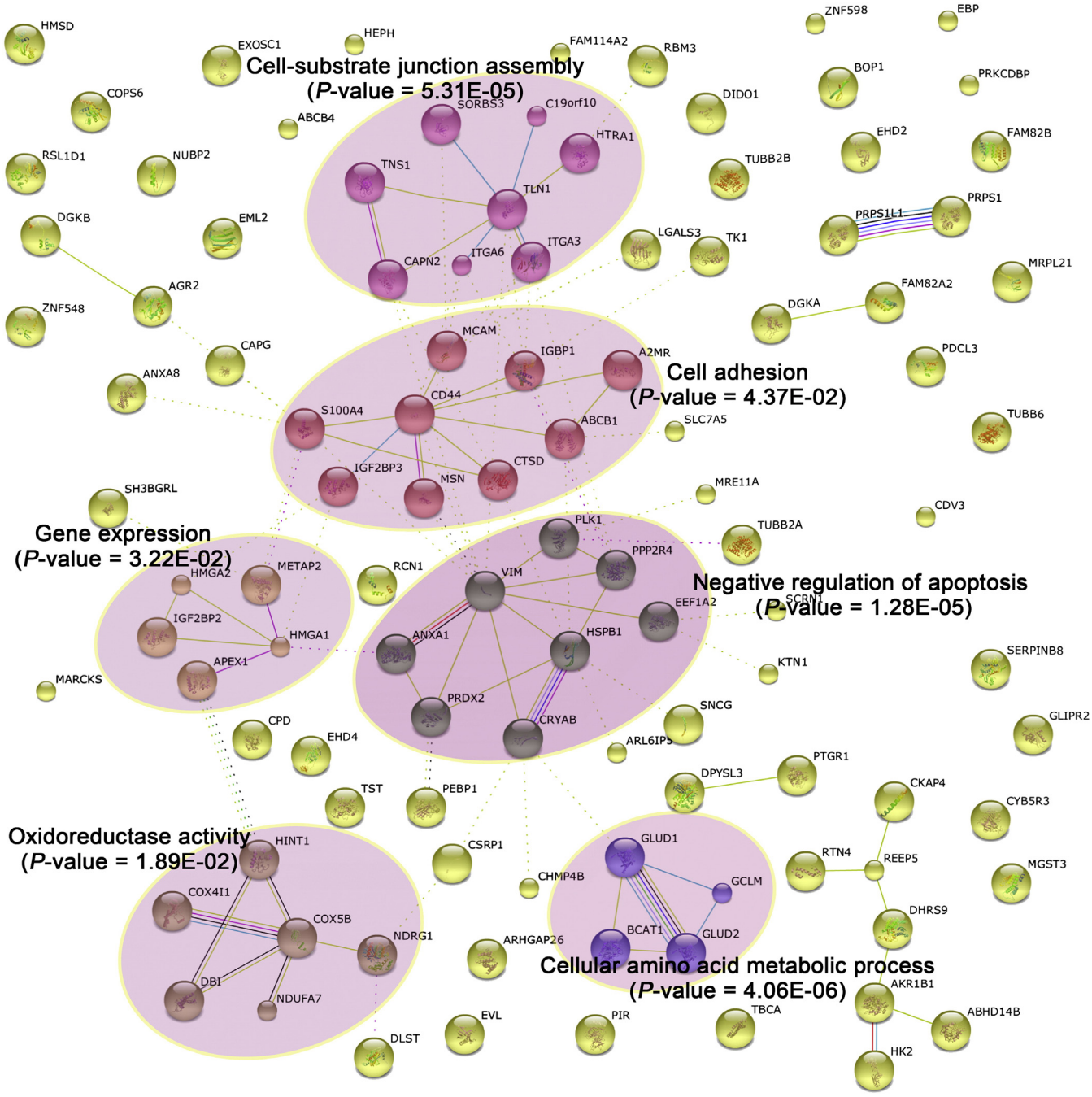

Fig. 3 – Functional protein complexes in CD146-induced EMT. The interactions between the 103 identified proteins were obtained from STRING, which formed six major modules after clustering by K-means (pink clouds). The functional annotation of the six major modules was analyzed by DAVID.

process of an EMT. Our previous study revealed that CD146 interacted with moesin protein resulting in melanoma cell migration [24], providing a striking positive control for our SILAC analysis. Other interaction subgroups provided potential connections of CD146 to a wide range of biological functions, including cell-substrate assembly, negative regulation of apoptosis, gene expression, cellular amino acid metabolic process, and oxidoreductase activity.

3.6. Estrogen receptor constitutes a putative central regulatory node during CD146-induced EMT

Transcriptional repression of the key EMT marker E-cadherin is a fundamental event during the EMT process [3]. We therefore continued our IPA-based analysis of the 103 identified proteins to search for candidate transcription regulators involved in CD146-induced EMT. As shown in Table 2, the estrogen receptor

Table 2 – Selected transcription regulators in CD146-induced EMT.

Transcription regulator	Predicted activation state	Regulation z-score	P-value of overlap	Target molecules in data set	Molecular type
Estrogen receptor	Inhibited	−2.354	6.39E−03	ANXA1, CAPG, CD44, ITGA3, MSN, and VIM	Group
PGR	NA	1.761	2.32E−03	CAPN2, CD44, ITGA6, NDRG1, and SERPINB8	Ligand-dependent nuclear receptor
TP53	NA	0.717	8.33E−03	ABCB1, ABCB4, ANXA1, CTSD, DGKA, HK2, LGALS3, NDRG1, PLK1, and S100A4	Transcription regulator
CEBPA	NA	−0.173	1.89E−02	AKR1B1, ANXA1, EEF1A2, and TUBB2A	Transcription regulator
KDM5B	NA	−1.841	1.86E−03	ARL6IP5, CD146, PIR, PRPS1, and TUBB2A	Transcription regulator
Ap1	NA	NA	3.36E−02	S100A4 and SNCG	Complex
SPDEF	NA	NA	1.20E−02	ITGA3, ITGA6, and VIM	Transcription regulator
HSF1	NA	NA	1.25E−02	ABCB1 and CRYAB	Transcription regulator
ASCL2	NA	NA	1.80E−02	CTSD	Transcription regulator
ZNF148	NA	NA	3.57E−02	VIM	Transcription regulator
MSX2	NA	NA	1.80E−02	VIM	Transcription regulator
SP1	NA	NA	3.13E−02	HINT1, HK2, HMGA1, SNCG, and VIM	Transcription regulator
TWIST2	NA	NA	7.84E−03	CD44 and VIM	Transcription regulator
YBX1	NA	NA	4.44E−02	ABCB1	Transcription regulator
KLF1	NA	NA	4.44E−02	CD44	Transcription regulator
KHDRBS1	NA	NA	1.80E−02	CD44	Transcription regulator
SNAI2	NA	NA	2.78E−03	ITGA3 and VIM	Transcription regulator
MEOX2	NA	NA	9.04E−03	LRP1	Transcription regulator
SMAD3	NA	NA	2.79E−02	S100A4 and VIM	Transcription regulator
MYCN	NA	NA	4.79E−05	APEX1, HK2, HMGA1, and MRE11A	Transcription regulator
BRCA1	NA	NA	4.59E−02	CTSD and PLK1	Transcription regulator
SMARCA4	NA	NA	4.46E−02	AGR2, CD44, ITGA3, and LGALS3	Transcription regulator
PA2G4	NA	NA	9.04E−03	AGR2	Transcription regulator
CTNNB1	NA	NA	2.69E−02	CD44, HTRA1, LGALS3, and RCN1	Transcription regulator
MYC	NA	NA	2.87E−04	APEX1, BCAT1, GCLM, HK2, HSPB1, and MRE11A	Transcription regulator

(ER) was the most significantly inhibited transcriptional regulator, to result in the upregulation of ANXA1, GAPG, CD44, ITGA3, MSN and VIM in CD146-induced EMT processes. Two key EMT transcription factors Twist 2 and Snai2 (also known as Slug) were shown to up-regulate CD44, ITGA3 and VIM.

Through a detailed analysis based on previously published work, we found that a further 14 of the 103 identified proteins were associated with the ER signaling, revealing its potential role in CD146-induced EMT (Table S3). 9 out of those 14 proteins were up-regulated in a CD146-dependent manner. They were negatively regulated by an ER signaling, or had negative correlations with ER in breast cancers. For example, IGF-II mRNA-binding protein 3 (IMP3), which is associated with triple-negative breast cancer, is repressed by ER-β [25]. Correspondingly, the 5 down-regulated proteins were either up-regulated by the ER signaling or positively associated with ER in breast cancers. For instance, Anterior gradient protein 2 (AGR2) is induced by estrogen and is associated with ER-α expression in breast cancers [26,27]; cathepsin D, an estrogen-stimulated expression protein, is highly expressed in epithelial breast cancers [28].

We further used IPA to determine whether the 103 identified proteins could be mapped to specific functional regulatory pathway networks. As shown in Fig. 4, the signal network with the highest significance corresponded to cancer, cell-to-cell signaling and interaction, as well as gastrointestinal disease. The NF-κB, AKT and P38 MAPK pathways, which have been found previously to be associated with CD146 [9,29,30], were present in this network, indicating that our SILAC system generated reliable data sets. Crucially, this network revealed that ER was a central regulatory node, which was predicted to regulate the ERK pathway and to be regulated by the NF-κB pathway. Additional signaling networks of interest corresponded to cell death, DNA replication, recombination and repair, and cancer (Fig. S4A); lipid metabolism, molecular transport, and small molecule biochemistry (Fig. S4B); as well as cellular movement and cell morphology (Fig. S4C).

In summary, our IPA-based analysis generated the complex functional networks and identified the possible transcription regulators that mediated CD146-induced EMT. Specifically, our results showed that ER signaling was significantly inhibited during this process, providing evidences that ER might possess the function of a central regulatory node.

3.7. ER-α expression is repressed in CD146-induced EMT

A critical question arising from our IPA-based analysis was, in what manner ER signaling was inhibited during the CD146-induced EMT process. Previously, CD146 was found to be associated with an ER-negative status and a TNBC phenotype in breast cancers [6,19]. We therefore wanted to investigate if downregulation of the ER resulted in the inhibition of ER signaling in CD146-induced EMT.

To address this issue, we focused on the expression of ER-α, the main isoform of ER with high importance in breast cancer progression. RNA was extracted from Mock, B10 and A5 cell samples and analyzed using semi-quantitative RT-PCR. As shown in Fig. 5A, ER-α mRNA was drastically reduced in both CD146-expressing B10 and A5 cells, but was present at high levels in Mock cells. This result was consistent with our Affymatrix gene chip data (Microarray, B10/Mock, 0.003-fold

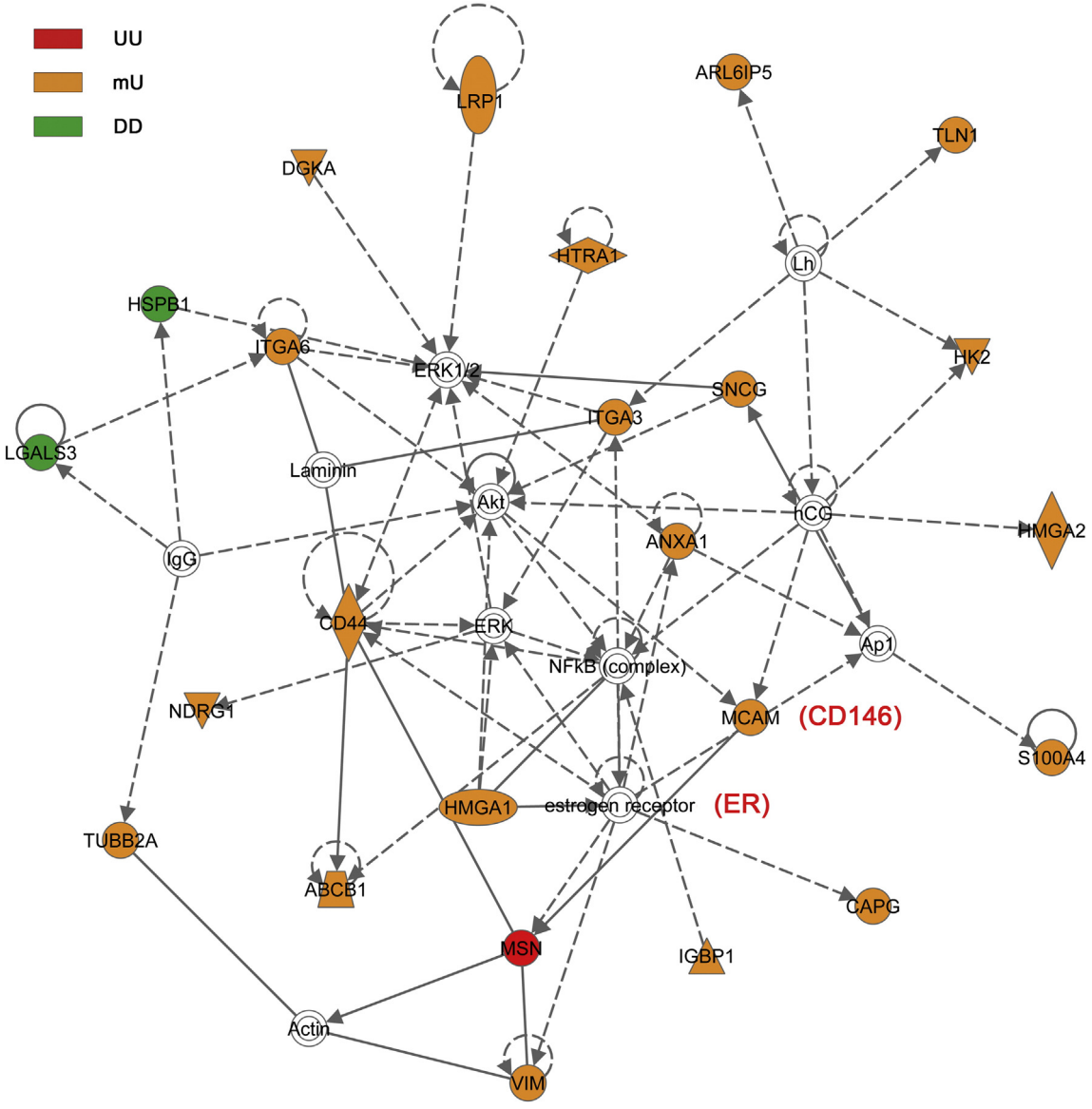

Fig. 4 – Estrogen receptor constitutes a putative central regulatory node during CD146-induced EMT. The highest-ranked signal network as revealed by Ingenuity Pathway Analysis (IPA) of the 103 identified proteins was predominately associated with cancer, cellular movement and gastrointestinal disease. Proteins indicated in orange were up-regulated only in A5 cells (mU), proteins indicated in red were up-regulated both in B10 and in A5 cells (UU), proteins indicated in yellow–green were down-regulated only in A5 cells (mD), and proteins indicated in green were down-regulated both in B10 and in A5 cells (DD) proteins indicated as white circles are those identified from the IPA Knowledge Base. The shapes are indicative of the molecular class (i.e. protein family). Lines connecting the molecules indicate molecular relationships. In detail, dashed lines indicate indirect interactions, and solid lines indicate direct interactions. The style of the arrows indicates specific molecular relationships and the directionality of the interaction (A acts on B).

change; A5/Mock, 0.002-fold change). Because no information was available for ER-α protein expression in our SILAC data, we analyzed ER-α protein levels for all the three cells by western blotting. In agreement with our mRNA analysis, we found that ER-α protein was also not detected in either B10 or A5 cells (Fig. 5B). Additionally, the repression of ER-α in cells that underwent CD146-induced EMT was confirmed by immunofluorescence. As shown in Fig. 5C, while Mock cells exhibited strong nuclear staining for ER-α, no nuclear signal was detected in B10 and A5 cells.

3.8. ER-α mediates the CD146-induced EMT process

We further investigated whether the repression of ER-α was responsible for CD146-induced EMT in breast cancer cells. Repression of ER-α in breast cancer cells has been shown to decrease E-cadherin expression, disrupt epithelial phenotype and promote cell invasive behaviors [31]. The inverse correlation between ER-α and CD146, as well as the EMT phenotype in Mock, B10 and A5 cells suggested that CD146 might inhibit the epithelial phenotype of breast cancer cells by repressing ER-α expression.

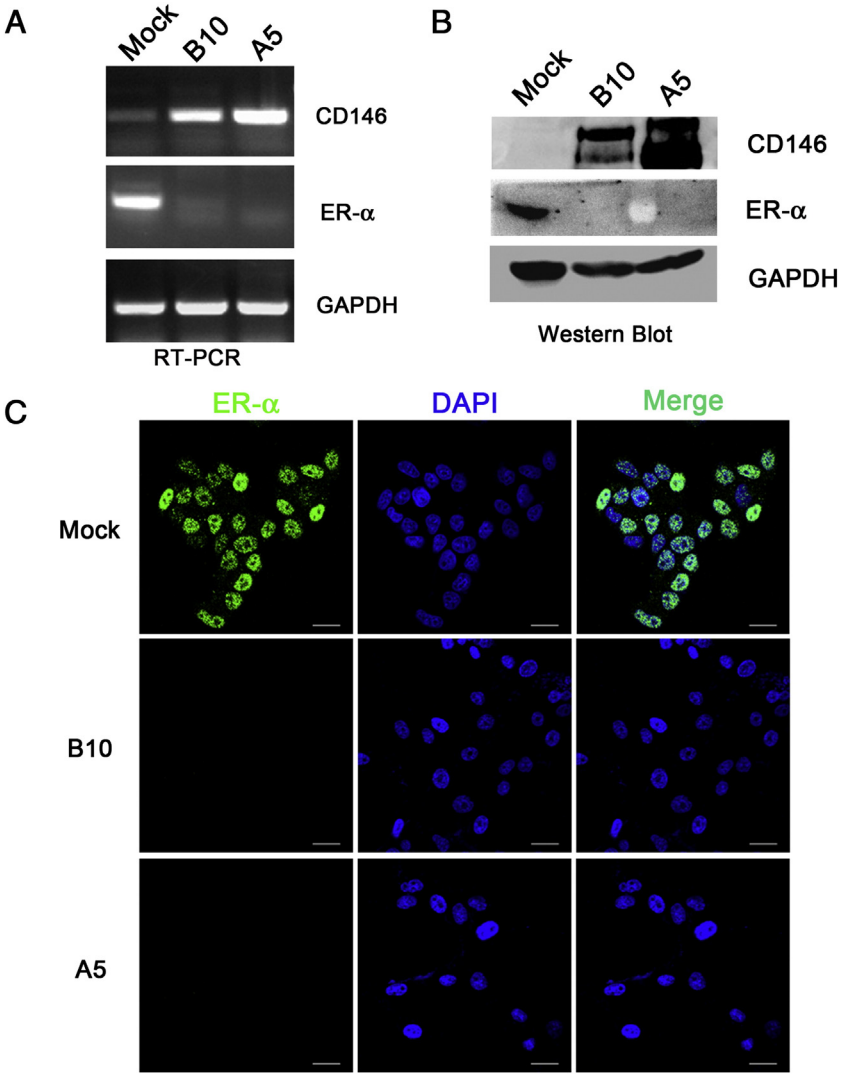

Fig. 5 – ER-α expression is repressed in CD146-induced EMT. (A) RT-PCR analysis of ER-α mRNA level in Mock, B10 and A5 cells. (B) Western blotting analysis of ER-α protein level in Mock, B10 and A5 cells. (C) Immunofluorescence analysis of ER-α expression in Mock, B10 and A5 cells. DAPI was used for nuclear staining. Scale bar, 20 μm.

To test this hypothesis, we re-expressed ER-α in CD146-expressing A5 cells with an ER-α negative status. As anticipated, we observed that the key epithelial marker E-cadherin was re-expressed, while the mesenchymal marker vimentin was down-regulated by about 30% as a consequence of ER-α re-expression (Fig. 6A–B). Interestingly, we also observed that CD146 was down-regulated by approximately 50% relative to its original levels, indicating a possible reciprocal regulation between ER-α and CD146 in breast cancer cells. Most importantly, ER-α re-expression significantly inhibited the migratory and invasive behavior of A5 cells (Fig. 6C–D), demonstrating that an increase in ER-α expression was able to reverse the CD146-induced EMT process.

The hallmark event of an EMT process is the downregulation of the key epithelial maker E-cadherin. A number of EMT pathways converge on EMT key transcription factors to inhibit E-cadherin transcription to initiate an EMT process. Previously, overexpression of CD146 was found to inhibit E-cadherin transcription via Slug [6]. Since we observed that both the E-cadherin protein (Fig. 6A) and its transcript (Fig. 6F) increased after ER-α was re-expressed in A5 cells, we further investigated whether Slug expression was changed upon this treatment. As shown in Fig. 6E–F, both RT-PCR and western blotting analysis showed that Slug expression was down-regulated when ER-α was re-expressed in A5 cells, indicating that Slug was negatively regulated by ER-α signaling. Taken together, these data demonstrated that ER-α mediated CD146-induced EMT process through the repression of the EMT key transcription factor Slug, providing further insights into the mechanisms behind the reverse correlation between CD146 and ER as observed in the clinic.

4. Discussion

Epithelial to mesenchymal transition (EMT) describes a complex process in which immotile epithelial cells lose their tight cell to cell junctions and acquire a migratory mesenchymal

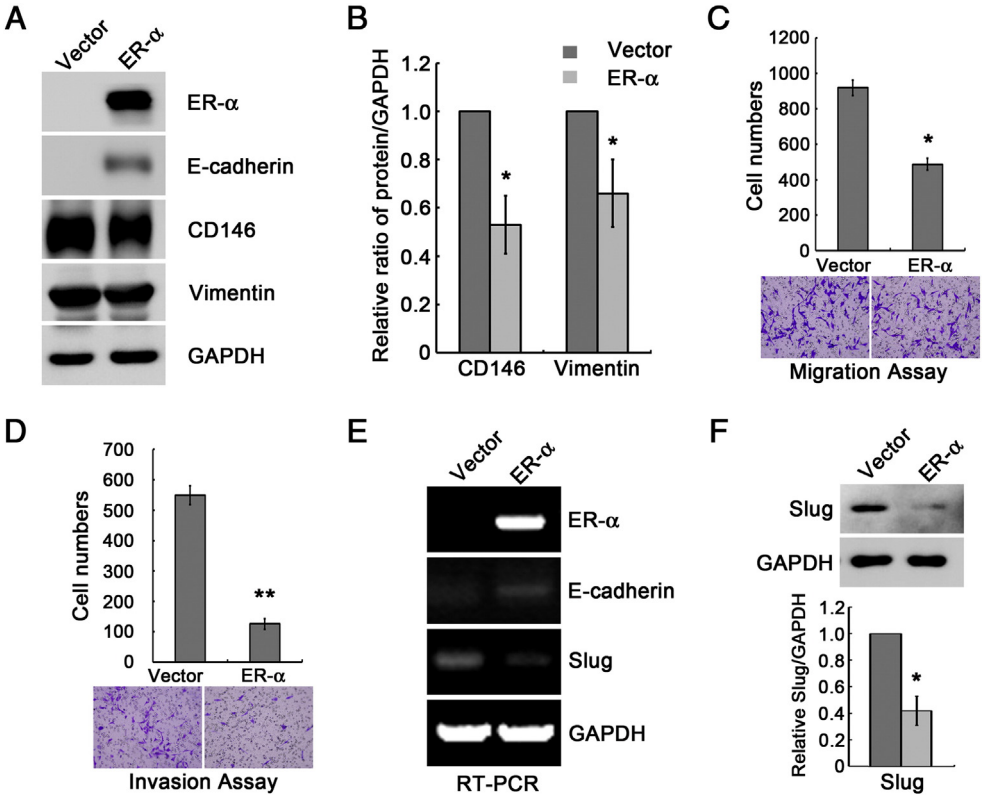

Fig. 6 – ER-α mediates the CD146-induced EMT process. (A) Western blotting analysis of ER-α, E-cadherin, CD146 and vimentin expression in A5 cells after ER-α was re-expressed. (B) Quantification of CD146 and vimentin expression in A5 cells after ER-α was re-expressed. *P < 0.05, compared with vector-transfected A5 cells. (C–D) Migration and invasion assays of A5 cells after ER-α re-expression. Data were collected from 3 wells; *P < 0.05 and **P < 0.01 compared with empty vector-transfected A5 cells. A representative image is shown under each graph. (E) RT-PCR analysis of the mRNA levels of ER-α, E-cadherin and EMT key transcription factor Slug in A5 cells after ER-α was re-expressed. (F) Western blotting analysis (upper panel) and quantifications (lower panel) of the protein level of Slug in A5 cells after ER-α re-expression. *P < 0.05, compared with empty vector-transfected A5 cells.

phenotype [1]. Originally identified during embryonic development, EMT is now known to play a critical role in organ fibrosis as well as during tumor progression. While a number of EMT inducers have been identified in the past two decades, including membrane receptors, intracellular molecules and external agents, few proteomic studies have focused on the complex molecular events and signaling networks initiated by each individual EMT inducer, and in different cellular contexts.

In this study, we carried out in-depth systems analysis of breast cancer cells that underwent EMT mediated by a novel EMT inducer CD146. As a result, we identified extensive morphological and biochemical changes in cell adhesion, negative regulation of apoptosis process and cell-to-cell junction. Although several EMT studies have used proteomics to gain new insights into the molecular events occurring at the protein level, these have been primarily based on 2-DE methodology. The disadvantage of these methods lies in the low detection limit as well as in the limited sample capacity, which only allows for monitoring of a few hundred proteins present at high cellular abundance [32–36]. In an attempt to systematically reveal novel EMT effectors and mechanisms, we for the first time implemented a triple-SILAC strategy to monitor protein expression profiles during the CD146-induced EMT process, which greatly increased the number of identified proteins, amounting to 2293 proteins in total, and 103 proteins with altered abundances that correlated with CD146 expression. More importantly, our triple-SILAC strategy based on moderate to high CD146 expression levels efficiently excluded unwanted proteins appearing, possibly due to individual clone differences, thus greatly reducing the number of false positive and negative signals. We ultimately used the 103 identified proteins as a starting point to generate functional interaction and signal networks based on system biology. Most notably, this strategy identified the estrogen receptor group as a central regulatory node during CD146-induced EMT.

Estrogen receptors (ERs) are members of the superfamily of nuclear hormone receptors, whose activities are crucial for the growth of mammary epithelial cells and breast cancer cells [37,38]. So far two isoforms of estrogen receptor (ER-α and ER-β) have been described, of which ER-α is the most important and the most thoroughly studied one. The interactions between ER-α and its main ligand estradiol (E2) promote their dimerization and nuclear translocation, where it acts as a transcriptional factor, regulating the transcription of various target genes [38].

In this manner, ligand-activated ER-α sets off a complex series of gene activations and biological functions in breast cancer cells. Our IPA-based analysis revealed that ER was the most significantly inhibited transcriptional regulator during the CD146-induced EMT process. Besides, we observed that 14 of the 103 identified proteins were associated with ER signaling in breast cancers, suggesting an important regulatory role of ER. For instance, cathepsin D, an estrogen-induced lysosomal protease that is overexpressed and hypersecreted by epithelial breast cancers, plays an essential role in epithelial cancer cell proliferation, fibroblast outgrowth and angiogenesis [28]. Besides these well-known biological processes associated with ER signaling, our study showed that CD146 provided a missing link between ER signaling and EMT. Overexpression of CD146 in MCF-7 cells diminished the expression of ER-α and initiated an EMT. Re-expression of ER-α in CD146-overexpressing MCF-7 A5 cells reversed their mesenchymal phenotypes and down-regulated Slug. Previous studies showed that when ER-α was knocked down in MCF-7 cells, the Slug repressor increased, E-cadherin decreased, and cells became spindly and invasive, all of which were consistent with our observations [31,39]. Ye et al. reported that ER-α suppressed the transcription of Slug via direct formation of a co-repressor complex with HDAC1 and N-CoR, or via indirect inactivation of GSK3β through PI3K/AKT [39], providing a strong platform for our proteomics and functional studies presented here. However, a number of questions still remain to be answered. For example, how could CD146, a cell adhesion molecule regulate ER-α expression? Our previous work showed that CD146 was involved in the NF-κB pathway [9,29]. A recent study reported that RelB NF-κB reciprocally inhibited ER-α synthesis via Blimp1 in breast cancer cells [40]. Based on these observations, we wonder whether CD146 could decrease ER-α expression via the NF-κB pathway, and this possible link certainly warrants further investigation.

In order to successfully metastasize and recur, tumor cells must have the potential of self-renewal and resistance to chemotherapy, probably through transforming into cancer stem cell-like cells. Our previous studies showed that breast cancer cells that underwent CD146-dependent EMT acquired some breast cancer stem cell-like properties, including a $CD24^{low}/CD44^{high}$ expression pattern and an increased capability of mammosphere formation [6], though the underlying mechanism remained unknown. In our SILAC assay, we confirmed that the cancer stem cell marker CD44 was up-regulated in breast cancer cells that underwent CD146-induced EMT. In addition, we identified another two candidate proteins that might be responsible for breast cancer stem cell-like properties induced by CD146. HMGA2, also known as the high-mobility group AT-hook 2 or HMGI-C, was found to be up-regulated in CD146-induced EMT. HMGA2 belongs to a family of nuclear factors that bind to AT-rich DNA sequences, which contributes to the transcriptional regulation of target genes [41]. HMGA2 has been shown to maintain the multipotency of cancer stem cells, and therefore may present a novel stem cell marker in breast cancer [42]. HMGA2 mediates E2F1 activity to promote tumorigenesis in a transgenic HMGA2 mouse model. It also acts as a downstream effector of the TGF-β signal pathway, possibly to initiate the EMT process [43]. The second candidate protein, αB-crystallin, also known as HSPB5, is a member of the heat shock protein family. αB-Crystallin displays anti-apoptotic properties and is tumorigenic when expressed in cancer cells. This protein has been shown to mediate several steps of the apoptosis pathway, such as binding of pro-apoptotic protein Bax, Bcl-xS [44] and p53 [45] to prevent their mitochondrial translocation, or inhibiting the activation of pro-caspase 3 [46]. Thus, αB-crystallin appears to be a major component in the processes leading to chemotherapy resistances in cancer cells and could therefore be considered to present an important potential therapeutic target. These observations would provide enough clues for exploring the underlying mechanisms between CD146-induced EMT and breast cancer stem cells.

It is a well-known fact that a solid tumor always displays enhanced, autonomous, or even unusual metabolic activities compared with its surrounding normal tissue. In our proteomics analysis, we also observed evidences of altered nutrient and energy metabolism in breast cancer cells during the CD146-induced EMT process. Two members of glutamate dehydrogenase (GLDH), GLUD1 and GLUD2, were found to be up-regulated in CD146-expressing cells. GLDH is a ubiquitously expressed enzyme that locates in the mitochondrial matrix, where it plays a central role in carbon and nitrogen metabolism. GLDH determines the metabolism rate of glutamate and other nonessential amino acids, and can be regulated by a series of factors, including allosteric effects, posttranslational modifications and others [47]. Yang et al. reported that the deprivation of glucose or, alternatively the inhibition of the AKT pathway in glioblastoma cells increases the activity of glutamate dehydrogenase, rendering cells dependent on glutamine to sustain viability under low glucose condition [48], an observation that directly links GLDH to cancer cell metabolism. Additionally, another mitochondrial protein COX4I1 was found to be down-regulated during CD146-induced EMT. COX4I1, also known as cytochrome oxidase subunit 4 isoform 1, belongs to the cytochrome c oxidase family. COX4I1, as well as another member of the same family, namely COX4I2, use oxygen as the terminal electron acceptor in the electron transport chain [49]. Earlier reports indicate that COX4I1 is down-regulated, while COX4I2 is up-regulated upon induction of hypoxia-induced factor (HIF) under hypoxia condition, resulting in an increase in oxygen consumption [50]. In addition to well-known EMT features, including enhanced cell motility, cancer stem cell properties and chemotherapy resistance, could a switch in metabolic pathways be an additional hallmark that characterizes the EMT process? These new observations should provide useful clues for future analysis of a new role of CD146 in cancer cell metabolism.

Triple-negative breast cancer (TNBC) is the most malignant and lethal subtype of breast cancer due to its high invasiveness and resistance to currently available targeted therapies. Accounting for 17–25% of all breast cancer types, TNBC is characterized by a lack of expression of estrogen receptor (ER), progesterone receptor (PR) and ErBB2 (HER2) [51]. Two intriguing features of TNBC are their apparent EMT phenotype, as well as an observed enrichment of breast cancer stem cells, which endows TNBC cells with enhanced capabilities for both metastasis and resistance to chemotherapeutic treatment. Our previous studies revealed that CD146 was significantly associated with TNBC. Using a SILAC approach as described here, we succeeded in identifying the reciprocal regulatory relationship between CD146 and ER-α, providing evidences for the critical

role of ER-α in CD146-induced EMT. Furthermore, we identified proteins previously unknown to form the molecular basis for the associations observed between CD146-induced EMT and breast cancer stem cell-like properties. In conclusion, our data would provide sufficient evidences for future exploration of the mechanisms underlying the association between CD146 and TNBC in the clinic.

5. Conclusion

In this work, the implementation of a triple SILAC-based proteomic analysis of CD146-induced EMT in breast cancer cells showed that a number of proteins were significantly altered in response to CD146 overexpression. Differentially expressed proteins were identified (n = 103) and further analyzed using bioinformatics software (Ingenuity Pathway Analysis, DAVID and STRING). Our network analysis revealed that estrogen receptor (ER) was the most significantly inhibited transcription regulator during CD146-induced EMT, suggesting that it might act as a central regulatory node. Further experiments were performed and validated our hypothesis of ER-α mediated CD146-induced EMT process through the repression of the EMT key transcriptional repressor Slug. In conclusion, we gained important mechanistic insights into the molecular events and signal networks activated by CD146, which provided an explanation for the reverse correlation between CD146 and ER as observed in breast cancer samples in the clinic.

This work contains peptide identification and quantification by SILAC (Table S1), protein identification and quantification by SILAC (Table S2), a word document containing supplementary legends and references (Supplementary information), overexpression of CD146 induces EMT in breast cancer cells (Fig. S1), a histogram showing the frequency in changes of protein levels (Fig. S2), functional characterization of the 103 identified proteins analyzed by Ingenuity Pathway Analysis (Fig. S3), Ingenuity Pathway Analysis of significantly associated functional networks based on the 103 identified proteins (Fig. S4) and the involvement of the identified differently expressed proteins in the estrogen receptor signaling (Table S3). All our raw data (including mass spectrometry data, protein identification data and microarray data) can be downloaded in PeptideAtlas (PASS00389). Supplementary data related to this article can be found online at http://dx.doi.org/10.1016/j.jprot.2014.03.033.

Transparency document

The Transparency document associated with this article can be found, in the online version.

Acknowledgment

This work was partly supported by grants from the National Natural Science Foundation of China (91329102, 81272409, 31300729, 81371330 and 81371025) and the National Basic Research Program of China (973 program) (2011CB915502).

REFERENCES

[1] Thiery JP, Acloque H, Huang RY, Nieto MA. Epithelial–mesenchymal transitions in development and disease. Cell 2009;139:871–90.
[2] Polyak K, Weinberg RA. Transitions between epithelial and mesenchymal states: acquisition of malignant and stem cell traits. Nat Rev Cancer 2009;9:265–73.
[3] Perl AK, Wilgenbus P, Dahl U, Semb H, Christofori G. A causal role for E-cadherin in the transition from adenoma to carcinoma. Nature 1998;392:190–3.
[4] Yang J, Weinberg RA. Epithelial–mesenchymal transition: at the crossroads of development and tumor metastasis. Dev Cell 2008;14:818–29.
[5] Shtutman M, Levina E, Ohouo P, Baig M, Roninson IB. Cell adhesion molecule L1 disrupts E-cadherin-containing adherens junctions and increases scattering and motility of MCF7 breast carcinoma cells. Cancer Res 2006;66:11370–80.
[6] Zeng Q, Li W, Lu D, Wu Z, Duan H, Luo Y, et al. CD146, an epithelial-mesenchymal transition inducer, is associated with triple-negative breast cancer. Proc Natl Acad Sci U S A 2012;109:1127–32.
[7] Lehmann JM, Riethmuller G, Johnson JP. MUC18, a marker of tumor progression in human melanoma, shows sequence similarity to the neural cell adhesion molecules of the immunoglobulin superfamily. Proc Natl Acad Sci U S A 1989;86:9891–5.
[8] Yan X, Lin Y, Yang D, Shen Y, Yuan M, Zhang Z, et al. A novel anti-CD146 monoclonal antibody, AA98, inhibits angiogenesis and tumor growth. Blood 2003;102:184–91.
[9] Jiang T, Zhuang J, Duan H, Luo Y, Zeng Q, Fan K, et al. CD146 is a coreceptor for VEGFR-2 in tumor angiogenesis. Blood 2012;120:2330–9.
[10] Fritzsche FR, Wassermann K, Rabien A, Schicktanz H, Dankof A, Loening SA, et al. CD146 protein in prostate cancer: revisited with two different antibodies. Pathology 2008;40:457–64.
[11] Wu GJ, Varma VA, Wu MW, Wang SW, Qu P, Yang H, et al. Expression of a human cell adhesion molecule, MUC18, in prostate cancer cell lines and tissues. Prostate 2001;48:305–15.
[12] Wu Z, Li J, Yang X, Wang Y, Yu Y, Ye J, et al. MCAM is a novel metastasis marker and regulates spreading, apoptosis and invasion of ovarian cancer cells. Tumour Biol 2012;33:1619–28.
[13] Aldovini D, Demichelis F, Doglioni C, Di Vizio D, Galligioni E, Brugnara S, et al. M-CAM expression as marker of poor prognosis in epithelial ovarian cancer. Int J Cancer 2006;119:1920–6.
[14] Kristiansen G, Yu Y, Schluns K, Sers C, Dietel M, Petersen I. Expression of the cell adhesion molecule CD146/MCAM in non-small cell lung cancer. Anal Cell Pathol 2003;25:77–81.
[15] Liu WF, Ji SR, Sun JJ, Zhang Y, Liu ZY, Liang AB, et al. CD146 expression correlates with epithelial–mesenchymal transition markers and a poor prognosis in gastric cancer. Int J Mol Sci 2012;13:6399–406.
[16] Bidlingmaier S, He J, Wang Y, An F, Feng J, Barbone D, et al. Identification of MCAM/CD146 as the target antigen of a human monoclonal antibody that recognizes both epithelioid and sarcomatoid types of mesothelioma. Cancer Res 2009;69:1570–7.
[17] Sato A, Torii I, Okamura Y, Yamamoto T, Nishigami T, Kataoka TR, et al. Immunocytochemistry of CD146 is useful to discriminate between malignant pleural mesothelioma and reactive mesothelium. Mod Pathol 2010;23:1458–66.
[18] Zeng GF, Cai SX, Wu GJ. Up-regulation of METCAM/MUC18 promotes motility, invasion, and tumorigenesis of human breast cancer cells. BMC Cancer 2011;11:113.

[19] Zabouo G, Imbert AM, Jacquemier J, Finetti P, Moreau T, Esterni B, et al. CD146 expression is associated with a poor prognosis in human breast tumors and with enhanced motility in breast cancer cell lines. Breast Cancer Res 2009;11:R1.
[20] Washburn MP, Wolters D, Yates III JR. Large-scale analysis of the yeast proteome by multidimensional protein identification technology. Nat Biotechnol 2001;19:242–7.
[21] Romijn EP, Yates III JR. Analysis of organelles by on-line two-dimensional liquid chromatography–tandem mass spectrometry. Methods Mol Biol 2008;432:1–16.
[22] Quan H, Peng X, Liu S, Bo F, Yang L, Huang Z, et al. Differentially expressed protein profile of renal tubule cell stimulated by elevated uric acid using SILAC coupled to LC–MS. Cell Physiol Biochem 2011;27:91–8.
[23] Cox J, Mann M. MaxQuant enables high peptide identification rates, individualized p.p.b.-range mass accuracies and proteome-wide protein quantification. Nat Biotechnol 2008;26:1367–72.
[24] Luo Y, Zheng C, Zhang J, Lu D, Zhuang J, Xing S, et al. Recognition of CD146 as an ERM-binding protein offers novel mechanisms for melanoma cell migration. Oncogene 2012;31:306–21.
[25] Samanta S, Sharma VM, Khan A, Mercurio AM. Regulation of IMP3 by EGFR signaling and repression by ERbeta: implications for triple-negative breast cancer. Oncogene 2012;31:4689–97.
[26] Innes HE, Liu D, Barraclough R, Davies MP, O'Neill PA, Platt-Higgins A, et al. Significance of the metastasis-inducing protein AGR2 for outcome in hormonally treated breast cancer patients. Br J Cancer 2006;94:1057–65.
[27] Fritzsche FR, Dahl E, Pahl S, Burkhardt M, Luo J, Mayordomo E, et al. Prognostic relevance of AGR2 expression in breast cancer. Clin Cancer Res 2006;12:1728–34.
[28] Liaudet-Coopman E, Beaujouin M, Derocq D, Garcia M, Glondu-Lassis M, Laurent-Matha V, et al. Cathepsin D: newly discovered functions of a long-standing aspartic protease in cancer and apoptosis. Cancer Lett 2006;237:167–79.
[29] Bu P, Gao L, Zhuang J, Feng J, Yang D, Yan X. Anti-CD146 monoclonal antibody AA98 inhibits angiogenesis via suppression of nuclear factor-kappaB activation. Mol Cancer Ther 2006;5:2872–8.
[30] Zheng C, Qiu Y, Zeng Q, Zhang Y, Lu D, Yang D, et al. Endothelial CD146 is required for in vitro tumor-induced angiogenesis: the role of a disulfide bond in signaling and dimerization. Int J Biochem Cell Biol 2009;41:2163–72.
[31] Fujita N, Jaye DL, Kajita M, Geigerman C, Moreno CS, Wade PA. MTA3, a Mi-2/NuRD complex subunit, regulates an invasive growth pathway in breast cancer. Cell 2003;113:207–19.
[32] Mathias RA, Chen YS, Wang B, Ji H, Kapp EA, Moritz RL, et al. Extracellular remodelling during oncogenic Ras-induced epithelial–mesenchymal transition facilitates MDCK cell migration. J Proteome Res 2010;9:1007–19.
[33] Mathias RA, Simpson RJ. Towards understanding epithelial–mesenchymal transition: a proteomics perspective. Biochim Biophys Acta 2009;1794:1325–31.
[34] Li LP, Lu CH, Chen ZP, Ge F, Wang T, Wang W, et al. Subcellular proteomics revealed the epithelial–mesenchymal transition phenotype in lung cancer. Proteomics 2011;11:429–39.
[35] Zhou C, Nitschke AM, Xiong W, Zhang Q, Tang Y, Bloch M, et al. Proteomic analysis of tumor necrosis factor-alpha resistant human breast cancer cells reveals a MEK5/Erk5-mediated epithelial–mesenchymal transition phenotype. Breast Cancer Res 2008;10:R105.
[36] Chen YS, Mathias RA, Mathivanan S, Kapp EA, Moritz RL, Zhu HJ, et al. Proteomics profiling of Madin–Darby canine kidney plasma membranes reveals Wnt-5a involvement during oncogenic H-Ras/TGF-beta-mediated epithelial–mesenchymal transition. Mol Cell Proteomics 2011;10 [M110 001131].
[37] Brisken C, O'Malley B. Hormone action in the mammary gland. Cold Spring Harb Perspect Biol 2010;2:a003178.
[38] Stingl J. Estrogen and progesterone in normal mammary gland development and in cancer. Horm Cancer 2011;2:85–90.
[39] Ye Y, Xiao Y, Wang W, Yearsley K, Gao JX, Shetuni B, et al. ERalpha signaling through slug regulates E-cadherin and EMT. Oncogene 2010;29:1451–62.
[40] Wang X, Belguise K, O'Neill CF, Sanchez-Morgan N, Romagnoli M, Eddy SF, et al. RelB NF-kappaB represses estrogen receptor alpha expression via induction of the zinc finger protein Blimp1. Mol Cell Biol 2009;29:3832–44.
[41] Reeves R. Molecular biology of HMGA proteins: hubs of nuclear function. Gene 2001;277:63–81.
[42] Yu F, Yao H, Zhu P, Zhang X, Pan Q, Gong C, et al. let-7 regulates self renewal and tumorigenicity of breast cancer cells. Cell 2007;131:1109–23.
[43] Thuault S, Valcourt U, Petersen M, Manfioletti G, Heldin CH, Moustakas A. Transforming growth factor-beta employs HMGA2 to elicit epithelial–mesenchymal transition. J Cell Biol 2006;174:175–83.
[44] Mao YW, Liu JP, Xiang H, Li DW. Human alphaA- and alphaB-crystallins bind to Bax and Bcl-X(S) to sequester their translocation during staurosporine-induced apoptosis. Cell Death Differ 2004;11:512–26.
[45] Liu S, Li J, Tao Y, Xiao X. Small heat shock protein alphaB-crystallin binds to p53 to sequester its translocation to mitochondria during hydrogen peroxide-induced apoptosis. Biochem Biophys Res Commun 2007;354:109–14.
[46] Morrison LE, Hoover HE, Thuerauf DJ, Glembotski CC. Mimicking phosphorylation of alphaB-crystallin on serine-59 is necessary and sufficient to provide maximal protection of cardiac myocytes from apoptosis. Circ Res 2003;92:203–11.
[47] Smith TJ, Stanley CA. Untangling the glutamate dehydrogenase allosteric nightmare. Trends Biochem Sci 2008;33:557–64.
[48] Yang C, Sudderth J, Dang T, Bachoo RM, McDonald JG, DeBerardinis RJ. Glioblastoma cells require glutamate dehydrogenase to survive impairments of glucose metabolism or Akt signaling. Cancer Res 2009;69:7986–93.
[49] Denko NC. Hypoxia, HIF1 and glucose metabolism in the solid tumour. Nat Rev Cancer 2008;8:705–13.
[50] Fukuda R, Zhang H, Kim JW, Shimoda L, Dang CV, Semenza GL. HIF-1 regulates cytochrome oxidase subunits to optimize efficiency of respiration in hypoxic cells. Cell 2007;129:111–22.
[51] Anders CK, Carey LA. Biology, metastatic patterns, and treatment of patients with triple-negative breast cancer. Clin Breast Cancer 2009;9(Suppl. 2):S73–81.